Nanoscale

Accepted Manuscript

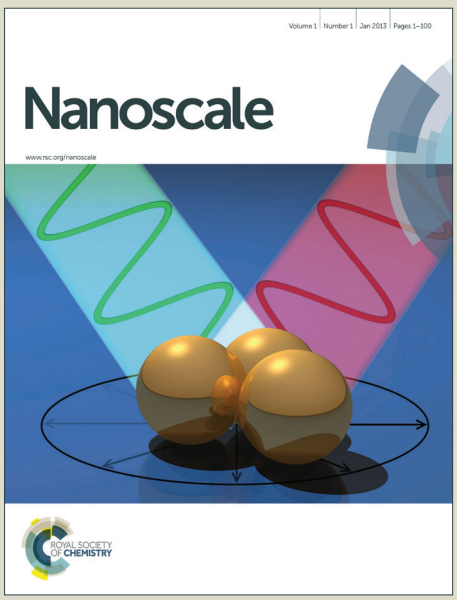

ROYAL SOCIETY OF CHEMISTRY

www.rsc.org/nanoscale

Nanoscale

RSCPublishing

ARTICLE

Non-destructive functionalisation for atomic layer deposition of metal oxides on carbon nanotubes: effect of linking agents and defects

Cite this: DOI: 10.1039/x0xx00000x

Received 00th January 2012,
Accepted 00th January 2012

DOI: 10.1039/x0xx00000x

www.rsc.org/

N. Kemnade,[a] C. J. Shearer,[a] D. J. Dieterle,[a] A. S. Cherevan,[a] P. Gebhardt,[a] G. Wilde[b] and D. Eder[a*]

The hybridisation of metal oxides and nanocarbons has created a promising new class of functional materials for environmental and sustainable energy applications. The performance of such hybrids can be further improved by rationally designing interfaces and morphologies. Atomic layer deposition (ALD) is among the most powerful techniques for the controlled deposition of inorganic compounds, due to its ability to form conformal coatings on porous substrates at low temperatures with high surface sensitivity and atomic control of film thickness. The hydrophobic nature of the nanocarbon surface has so far limited the applicability of ALD on CNTs. Herein we investigate the role of structural defects in CNTs, both intrinsic and induced by acid treatment, on coverage, uniformity and crystallinity of ZnO coatings. Furthermore, we demonstrate the potential of small aromatic molecules, including benzyl alcohol (BA), naphthalene carboxylic acid (NA) and pyrene carboxylic acid (PCA), as active nucleation sites and linking agents. Importantly, only PCA exhibits sufficiently strong interactions with the pristine CNT surface to withstand desorption under reaction conditions. Thus, PCA enables a versatile and non-destructive alternative route for the deposition of highly uniform metal oxide coatings onto pristine CNTs via ALD over a wide temperature range and without the typical surface corrosion induced by covalent functionalisation. Importantly, preliminary tests demonstrated that the improved morphology obtained with PCA has indeed considerably increased the hybrid's photocatalytic activity towards hydrogen evolution via sacrificial water splitting. The concept demonstrated in this work is transferable to a wide range of other inorganic compounds including metal oxides, metal (oxy)nitrides and metal chalcogenides on a variety of nanocarbons.

Introduction

Nanocarbon-inorganic hybrid materials constitute an exciting new class of functional materials with great potential in environmental and sustainable energy applications, including photovoltaic and photocatalysis[1, 2], chemical and biosensors[3], energy storage[4] and energy conversion[5]. In contrast to nanocarbon composites, where a small percentage of the nanocarbon (carbon nanotube (CNT), graphene, fullerene) is dispersed in a polymeric or ceramic matrix, the inorganic compound in the nanocarbon hybrid is deposited onto the nanocarbon's surface in a way that enables ready access to a large specific surface area of the active component as well as to a large interfacial area, thus introducing the interface as a powerful parameter. The beneficial effects in nanocarbon hybrids arise from the nanocarbon's unparalleled electronic properties[6], which can facilitate charge transport/extraction at the interface, as well as the excellent thermal transport properties of nanocarbons[7], which can induce interfacial energy transfer and so stabilize unique/uncommon crystal phases and even alter the activity and selectivity of catalytic reactions.[8] Understandably, these effects are further enhanced by purposefully engineering the interfaces[9], i.e. by facilitating strong coupling between the two components and increasing the interfacial area.

Our aim is to gain fundamental understanding of the nature and extent of interfacial processes in nanocarbon-inorganic hybrids by designing suitable model systems. Atomic layer deposition (ALD) is a very promising technique for the deposition of the inorganic component, due to its ability to form conformal coatings on porous substrates at low temperatures with atomic control of film thickness, high surface sensitivity and the possibility to coat multi-component layers.[10, 11] Coverage and

uniformity of ALD deposited thin films strongly depend on the surface chemistry of the substrate. For the deposition of metal oxides, for example, the substrate typically needs to be hydrophilic. Nanocarbons are hydrophobic and thus require chemical functionalisation[12, 13]. So far, ALD has been employed predominantly using CNTs that were pre-modified through oxidative treatments such as with strong acids,[12] ozone,[14] plasma[15] and nitrogen dioxide[16]. However, such treatments are often time-consuming and generally do not allow sufficient control over type, number and location of functional groups[17]. In addition, covalent functionalisation leads to considerable corrosion of the nanocarbon's surface, severely altering their mechanical and electrical properties and thus reducing their potential applicability.[18] Apart from covalent functionalisation, there have been only very few alternative approaches using, for example, highly defective MWCNTs[19-22], reduced graphene oxide (RGO)[19-22] or N-doped CNTs[23].

A more promising route is the modification of pristine CNTs with non-distructive bifunctional linker molecules, whose aromatic functions adsorb on the CNT surface while a hydrophilic function provides active sites for the attachment of inorganic species. This concept has been successfully applied in wet-chemical coating of CNTs, e.g. via solvothermal or sol-gel processes, using a variety of linker molecules, such as benzyl alcohol[24]. However, applying this concept to gas phase deposition processes such as ALD is complicated by both high temperature and low pressure. The crystallinity and morphology of the deposited film strongly depends on the deposition temperature such that elevated temperatures (e.g. 100 – 300 °C are preferred for high quality coatings).[25] In addition, ALD operates at low pressures (e.g. 0.1-10 Torr) in order to facility high purity coatings. Consequently, the adsorption of linker molecules on the CNT surface must be sufficiently strong to withstand these process conditions.

In this work, we investigate the use of three different aromatic linkers, i.e. benzyl alcohol (BA), naphthalene carboxylic acid (NA) and pyrene carboxylic acid (PCA), which contain 1, 2, and 4 aryl groups, respectively. In addition, we use acid-treated CNTs and pristine CNTs with various defect concentrations and compare the coverage, uniformity and crystallinity of ZnO coatings with non-covalently modified CNTs. We also evaluated the hybrids' performance for photocatalytic hydrogen production via sacrificial water splitting. We focus on the deposition of ZnO, which is among the most important transition metal oxides in nanocarbon hybrids due to its optoelectronic, photocatalytic and fluorescent properties,[26] yet the concept demonstrated in this work is easily transferable to a wide range of other inorganic compounds including metal oxide, metal (oxy)nitrides and metal chalcogenides.

Experimental

CNT synthesis

Carbon nanotubes have been produced with a floating catalyst chemical vapour deposition method (FCCVD)[27], using a two stage horizontal tube furnace (type HZS, Carbolite, UK) and a custom-built temperature-controlled syringe injection inlet. In detail, a solution of 4 wt% ferrocene in toluene was continuously injected into a pre-heated (180 ^{o}C) inlet at a rate of 5.4 mL h^{-1} before being carried in an argon flow (400 mL min^{-1}) into the quartz reaction chamber that was heated at 760 ^{o}C. After a typical reaction time of 5 h, the reactor was cooled to room temperature and the CNTs were collected from the inner walls of the quartz tube.[28] Length and average outer diameter of the as-grown CNTs were 500-600 µm and around 80 nm, respectively. The specific surface area was determined by N_2 physisorption to be 30 m²/g according to BET.

Processing of CNTs

The as-grown CNTs were annealed at 1000 ^{o}C (*anCNT-1000*) in argon (400 mL min^{-1}) for 6 h to remove residual amorphous carbon and, for comparison, at 2100 °C (*anCNT-2100*) to additionally remove encapsulated iron catalyst residues and to anneal structural defects.[1] The D:G ratio in the Raman spectra (Figure 1b) decreased from 0.32-0.39 for as-grown and anCNT-1000 to 0.17 for anCNT-2100. Thermal analysis (Figure S1) further documents that the remaining weight, which stems from residual Fe_2O_3, was reduced from 7.9 to 2.6 %.

Acid-treated CNTs (*atCNT*) were prepared following a 2-step acid treatment procedure. Thermally annealed CNTs were first refluxed in 3 M HNO_3 for 10 h and subsequently sonicated in a solution of 3:1 H_2SO_4:HNO_3 for 3 hours at room temperature. The CNTs were diluted in H_2O, vacuum filtered and washed with H_2O until a neutral filtrate was obtained and finally dried overnight in an oven at 70 ^{o}C. Thermal analysis (Figure S2) in air reveals a weight loss from 100 to 500 °C of about 6.7%.

The use in ALD required for CNTs to be assembled into porous membranes ("bucky-paper", Fig. 1a) due to high vacuum conditions in the ALD chamber. In a typical reaction, 1.25 mg ml^{-1} anCNTs and atCNTs were dispersed in ethanol via sonication for 15 min and subsequently subjected to vacuum filtration. After drying at room temperature, the CNT membranes were peeled from the filter paper to produce mechanically stable "bucky-paper" with a specific surface area of 25 m²/g with a pore volume of ~ 0.05 cm^3g^{-1}.

For non-covalent functionalisation, the anCNT membranes were further processed with benzyl alcohol (*BA-CNT*), naphthalene carboxylic acid (*NA-CNT*) and pyrene carboxylic acid (*PCA-CNT*) via three methods: *Wet impregnation process*: 25mg CNTs were added to a solution of ethanol containing an excess of BA (0.4 µL mL^{-1}), NA (0.04 mg mL^{-1}) or PCA (0.04 mg mL^{-1}). After soaking for 15 min with the aid of sonication, the dispersion was vacuum filtered and the "bucky-paper" was slowly dried at room temperature. *CVD process* (only for NA and PCA): the anCNT-membrane was placed on top of a quartz crucible containing 3 mg of the linking agent and positioned inside a quartz tube within a tube furnace. The furnace was heated to 250 °C in flowing argon and kept at that temperature

for durations between 30 min and 4 h. *Hydrothermal process*: A solution of ethanol with BA (10 µL mL^{-1}), NA (1 mg mL^{-1}) or PCA (1 mg mL^{-1}) was filled into a small Teflon beaker and placed inside the Teflon liner of a typical autoclave (Parr Instrument Company, model 4749). The anCNT membrane was placed on top of the beaker to avoid direct contact with the solution. The autoclave was then heated to temperatures between 215 °C and 285 °C for 2 h.

Atomic layer deposition (ALD)

The CNT-membranes were placed inside the reaction chamber of a Savannah 100 ALD system (Cambridge Nanotech), which was kept purging in N_2 (20 sccm) for 10 min while reducing the pressure to 0.2 torr. The N_2 flow was subsequently reduced to 10 sccm before first water (oxygen source) and then the metal precursor (dimethylzinc) were injected into the chamber in pulses of 0.03 sec and 0.05 sec respectively. After each injection, the samples were exposed to each reactant for 10 sec before subjected to another purging of 15 s. The deposition temperature was varied between 90 °C and 200 °C and the injection cycle repeated between 20 and 300 times.

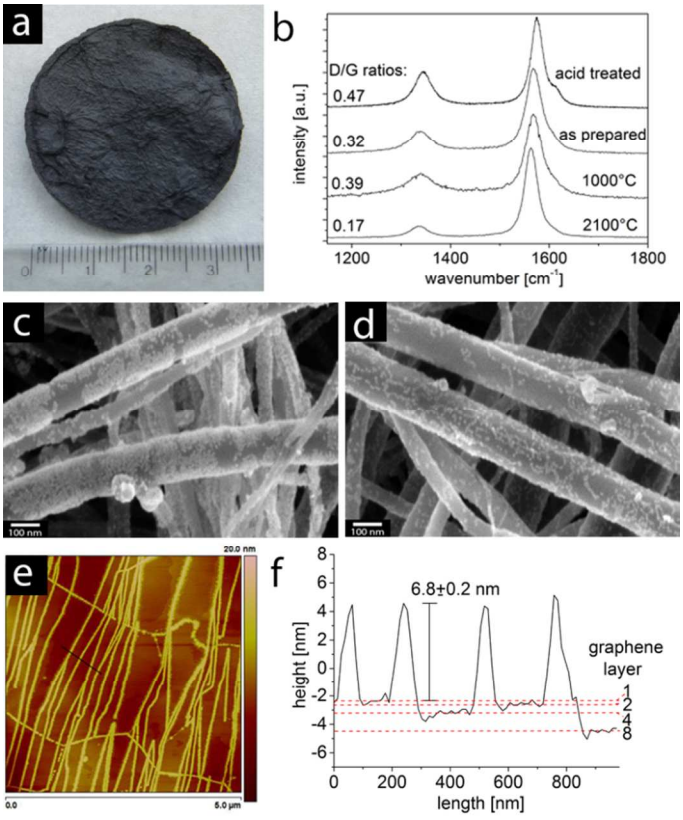

Figure 1. a) Digital photograph of a CNT "bucky-paper" used for ALD; b) Raman spectra and D/G ratios of acid-treated, as prepared and at 1000/2100°C annealed CNTs; c-d) SEM images of *anCNT-1000* and *an-CNT2100,* respectively, using 20 ALD cycles of ZnO; e) AFM characterisation of HOPG coated with 20 ALD cycles of ZnO (f) and a cross sectional height scan with graphitic layers indicated with red dotted lines.

Characterisation of hybrids

The morphology was characterised via scanning electron microscopy (SEM, Zeiss XB 1540 EsB) with an applied acceleration voltage of 2 kV and the use of a secondary electron detector, and via transmission electron microscopy (TEM, Zeiss Libra 200 FE) with 200 kV electron beam acceleration voltage. STEM images were recorded with a HAADF detector and a spot size of 1 nm. EDX was measured with a spot size of 4 nm (Fig S8). The samples were dispersed in EtOH and dropped onto Cu grids with a lacey(R) film.

The crystallinity of the deposited ZnO was determined by X-ray diffraction (XRD), using a RINT-Ultima III from Riguka with Cu K_α irradiation. Raman spectra were obtained by a Jobin Yvon Horiba LABRAM HR with a Nd:YAG-Laser (λ=532 nm), CCD and optical microscope (Olympus BX41). N_2-Physisorption was measured with a Micromeritics ASAP 2010 at 77 K. The total surface area was determined via the Brunauer-Emmett-Teller (BET) method and the pore volume via Barret-Joyner-Halenda (BJH).

A Dimension 3100 (Digital Instruments) was used in tapping mode under ambient conditions for atomic force microscopy (AFM) with a Tap300Al Silicon AFM probe. The thermogravimetric measurements were carried out on a TGA Q5000 (TA Instruments). The samples were filled in an Al_2O_3-crucible and stabilised isothermally at 40°C for 1h. A temperature ramp from 30 to 1000 °C with 5 K/min under N_2 was applied. For fluorescence measurements a Fluorolog 3 (Horiba Jobin Yvon) was used with a Xenon lamp and for the ZnO samples 325 nm were used as excitation wavelength.

Photocatalytic tests

The samples were tested in sacrificial water splitting for H_2 generation. In a typical experiment 16 mg of a ZnO-CNT hybrid membrane was dipped into 50 ml of water-methanol mixture (volume ratio of 1:4) placed in a top irradiation gas flow type reactor equipped with a quartz window. During the experiment the reaction media was constantly purged with Ar (99.998 % pure) to trap the reaction products and deliver them to the on line gas analyser (Emerson Process Management) that was used to quantify the amounts of generated H_2. The gas flow was controlled via a mass flow controller (MCC-Instruments). The detection limit for H_2 evolution in the applied system was 1 µmol h^{-1} with a maximum noise level of 0.3 µmol h^{-1}. UV-vis light source (Lumatec) equipped with a 200 W super pressure Hg lamp was used to deliver light to the reaction media in the wavelength range of 240-500 nm by means of an optical fibre. The photocatalysts were loaded with 0.5 wt% Pt via in situ photodeposition of H_2PtCl_6. Collected data (rate of H_2 production) was plotted against irradiation time.

Results and discussion

Atomic layer deposition of ZnO on pristine CNTs. The first task was to optimise sample preparation and process parameters. High vacuum and elevated temperatures typically

restrict the use of powdered CNTs for ALD. The deposition of CNTs on substrates, e.g. through drop-casting or spin-coating, is impractical as it prevents conformal coatings. The assembling of CNTs into highly porous membranes, known as "bucky-paper" (Fig. 1a), proved to be the most suitable sample preparation. It is important to note that the membranes require sufficient porosity, which can be achieved by varying type and concentration of the solvent as well as solvent evaporation rate. The best results were obtained when the CNTs were first dispersed and ultrasonicated in ethanol and subsequently slowly dried under reduced pressure, which provided membranes with voids of several hundreds of nanometers resulting in an apparent density of 0.15 cm^3/g. The quality of ALD coatings also depends on various process parameters, such as pulse duration, waiting and exposure time, and temperature, which need to be optimised for each materials system and setup. The exposure time had the most crucial effect on coating uniformity and yielded the best results at 10 sec.

ZnO was first deposited on non-functionalised CNTs for reference. Prior to the ALD process, any functional groups present on the CNTs were removed by thermal annealing at 1000°C and 2100 °C under inert atmosphere. SEM confirms the presence of ZnO nanoparticles on *anCNT-1000* (Fig. 1c) and *anCNT-2100* (Fig. 1d, Fig. S4). The nanoparticles are randomly distributed and often aggregated into large clusters. This suggests that the pristine CNT surface is not entirely inert and that presumably intrinsic defects in the sp^2 network provide nucleation sites. Detailed analysis with Raman spectroscopy revealed that the D:G ratio, which is indicative of sp^3-associated defects in the graphitic carbon walls, was lower for anCNT-2100 (~0.17) than for anCNT-1000 (~0.39). Therefore, the number of nucleation sites - and hence the number of ZnO nanoparticles is greatly reduced on *anCNT-2100*, in line with the SEM results which show significantly lower ZnO coverage.

In order to assess the potential of defects as nucleation sites, we investigated the deposition of ZnO nanoparticles (20 ALD cycles) on highly oriented pyrolytic graphite (HOPG) with atomic force microscopy (AFM). Figure 1e shows a typical surface of HOPG with flat areas separated by several sharp lines, which mark the steps between the graphene terraces. The height difference between the terraces varied from 0.4 to 2.8 nm, which correspond to 1 and 8 graphene layers, respectively. The standard deviation of the surface roughness was measured with 0.2 nm (Fig. S9). In the case of ZnO deposited on HOPG, the average height near these steps was considerably increased. The peaks in the line scan document the presence of ZnO nanoparticles, which seemingly follow the exact pattern of the freshly cleaved HOPG steps (Fig. S9). Importantly, no deposition of ZnO was observed on the flat, graphitic carbon surface. This indicates that the edges of the graphene layers (i.e. sp^3-type, resembling structural defects in CNTs) are more reactive than the graphitic (i.e. sp^2-type) basal areas of HOPG. Interestingly, the observed height of 6.8 nm for ZnO on HOPG was significantly larger than for the ZnO deposition on a Si substrate, which yielded a film thickness of only 4 nm with the same process conditions (determined by AFM). The calculated film thickness (i.e. particle size) for ZnO after 20 deposition cycles is 6.5, 5.3 and 8.4 nm for a growth in [100], [001], and [101] direction, respectively. Hence, in contrast to Si, the edge atoms in graphite have facilitated the growth of ZnO predominantly into the [100] direction. These results prove the reactivity of edge atoms and confirm that structural defects in nanocarbons can indeed act as potential nucleation sites and potentially alter the growth direction.

PRE-MODIFICATION OF CNTS VIA NON-COVALENT FUNCTIONALISATION. Low concentration and random distribution of intrinsic structural defects in CNTs typically prevent the deposition of homogeneous films with uniform thickness, as seen in Figure 1. Earlier concepts to improve the coating of CNTs (i.e. via wet-chemical techniques) have aimed to increase the number of nucleation sites by introducing functional groups, such as carboxyl- or hydroxyl groups, via covalent functionalisation (e.g. acid treatment). Figure 2a confirms that acid-treated CNTs (atCNTs, D:G = 0.47) have attracted more ZnO nanoparticles than thermally annealed CNTs. The coating, however, was not homogenous and often detached from the CNT surface. Therefore, we modified CNTs with aromatic linking agents using non-covalent (i.e. non-disruptive) interactions based on π-π stacking, which requires highly graphitic, defect-free CNT surfaces. In particular, we exposed anCNT-2100s to pyrene carboxylic acid (PCA) via three routes, i.e. wet impregnation in ethanol, CVD and hydrothermal process. The amount of adsorbed PCA was quantified by TGA (Fig. S3) and the surface coverage was calculated using 25 m^2/g as the specific surface area of the CNT membranes from BET measurements and 0.8 nm^2 as the adsorption cross-section of PCA. As shown in Table S1, wet impregnation yielded the smallest surface coverage of about 17 %. The apparent surface coverage was considerably larger when using CVD (68 %) as well as the hydrothermal process, in which the coverage increased with reaction temperature from 64 % to 117 % and 156 % for 215 °C, 255 °C and 285 °C, respectively. Figure 2f shows the desorption of PCA according to differential thermal gravimetry (DTG) and reveals two desorption peaks centered at around 200 °C and 350 °C. Considering that the desorption temperature is a measure for the strength of the interaction, the high-temperature peak can be associated with π-π interaction of the aromatic part of PCA with the nanocarbon surface, while the portion of PCA that desorbed at low temperature may correspond to weaker interactions, such as either vertically adsorbed molecules on the CNT surface or stacked PCA multi-layers[29]. This considering, the evolution of the low-temperature peak above 215 °C would indicate the completion of monolayer adsorption, and thus this temperature was chosen for all following experiments.

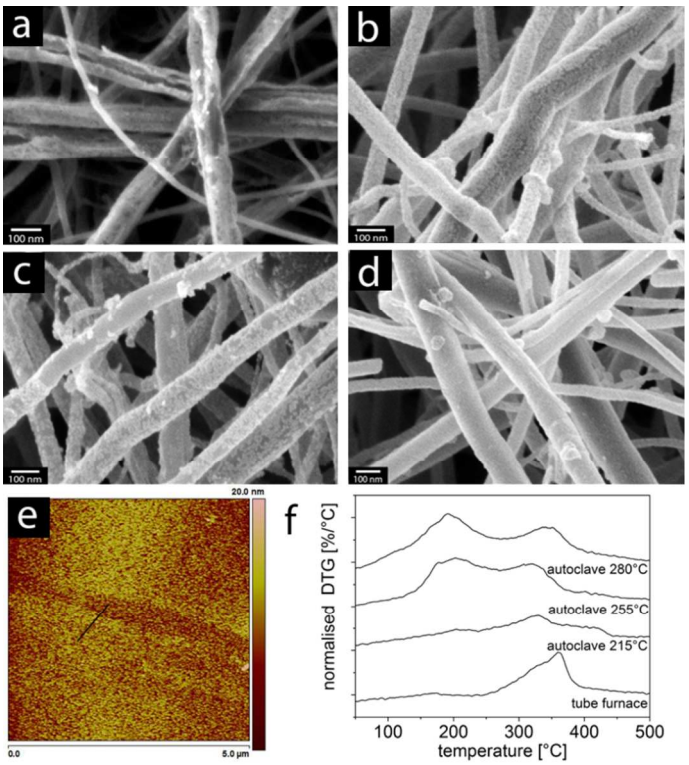

Figure 2. SEM images of CNTs coated with 20 ALD cycles of ZnO. a) coating on acid-treated CNTs; b) coating on CNTs functionalised with BA; c) coating on CNTs functionalised with NA; d) coating on CNTs functionalised with PCA. e) AFM measurements of HOPG functionalised with PCA and coated with 20 ALD cycles of ZnO; f) DTG *anCNT-1000* functionalised with PCA via solvothermal treatment at 215°C, 255°C, and 280°C.

Effect of non-covalent functionalisation on ZnO coatings. Figure 2b-d show SEM images of anCNT-2100s modified with BA, NA and PCA, respectively, and coated with ZnO at 90 °C using 20 injection cycles. In contrast to NA, the deposition of ZnO was clearly facilitated by BA and especially by PCA, which yielded a very dense and homogeneous coating (see SI, Fig. S4). The thickness of the coating was considerably more uniform than on acid-treated or annealed CNTs. For comparison, the deposition was carried out at higher temperatures (i.e. 200 °C), which is often chosen as it typically results in higher crystallinity of the deposited material[23]. PCA again enabled a dense and homogeneous coating, while only few ZnO particles were adsorbed in the case of BA and NA (Fig. S5-6).

These results confirm that the type of linker molecule is indeed crucial for obtaining uniform coatings. It is well known that the amount of π-electrons in the linker molecules and thus their interaction with the nanocarbon surface increases with the number of aromatic rings.[30] Consequently, the interaction with the CNT surface is considerably stronger for PCA (4 rings) than for NCA (2 rings) and BA (1 ring). Considering the aforementioned reaction conditions for ALD (i.e. high vaccum, elevated temperature), it is likely that the interaction of NA and BA with CNTs is not sufficiently strong so that the linkers may have simply desorbed during the coating process, thus limiting the amount of ZnO particles on the carbon's surface.

The potential of PCA was further tested with HOPG. Figure 2e shows that the ZnO nanoparticles were uniformly distributed over the entire surface of graphite in contrast to the aforementioned edge adsorption on pristine HOPG (Fig 1e, and line scan in Fig. S10). This confirms that PCA is a powerful linking agent for the deposition of metal oxides even under vacuum conditions at elevated temperatures.

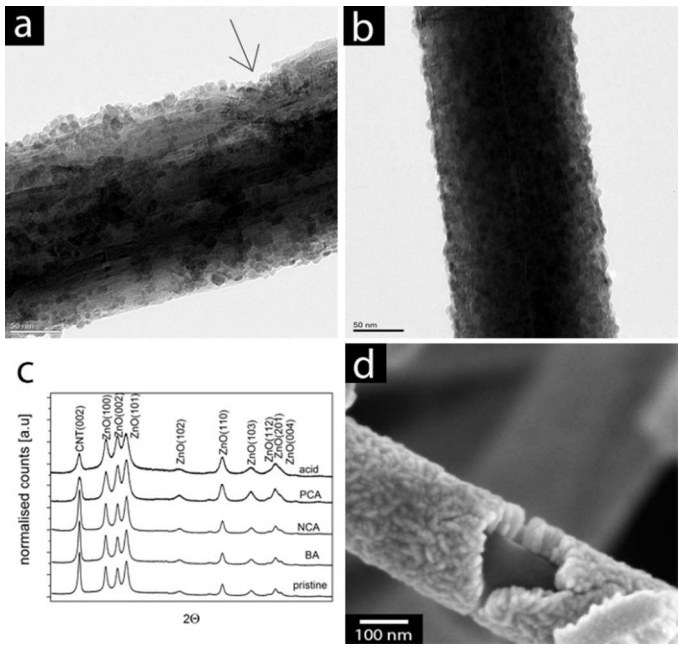

Figure 3. TEM images of acid treated CNTs, with an arrow indicating severe corrosion due to the acid treatment, (a) and *anCNT-2100* functionalised with PCA (b) coated with 20 ALD cycles of ZnO; c) comparison of XRD of ZnO films on CNTs facilitated by various functionalization methods; d) SEM image of *anCNT-1000* coated with 300 ALD cycles of ZnO.

X-ray powder diffraction (XRD) confirms further that the ZnO particles were crystalline in all samples (Fig. 3c). The peak at 26.1 ° corresponds to the (002) diffraction of multi-walled CNTs[31], while all other diffractions were assigned to the wurtzite structure of ZnO[32]. The relative intensity of the ZnO diffractions with respect to the (002) carbon diffraction (and thus the amount (and thus packing density, SI) of ZnO particles on the CNT surface) decreased in the order *PCA : atCNTs : BA : NA ~ anCNT2100*, which is in line with the SEM results (Fig. S4). The peak width of the ZnO diffractions further indicates that the crystal sizes varied with the type of linking agent. The average crystal size, calculated using Scherrer's equation[33, 34], was considerably smaller in the samples with PCA and on acid-treated CNTs (~7.5 nm) than with NA and BA (~ 10.5 nm) and on anCNTs (~ 11.5 nm). Although XRD suggests that the ZnO particles on PCA-modified and acid-treated CNTs were comparable in size, a closer look with TEM (Figure 3a,b) and STEM (Fig S7) revealed that the actual crystal sizes varied more widely on acid-treated CNTs (i.e. 3 to 13 nm) than with PCA (i.e. 6 to 9 nm). This confirms that PCA provided more uniformly distributed nucleation sites than the functional

groups introduced by acid-treatment. Furthermore, the TEM image documents the severe corrosion that the harsh acid-treatment had caused to several graphitic layers. The uniformity of the ZnO crystals was preserved even for very thick coatings, such as shown in Fig. 3d for 300 ALD cycles, which yielded elongated crystals with lengths of 60 nm. The width of the crystals was similar to those obtained with 20 cycles, thus confirming that PCA maintained its role as nucleation sites even for thick coatings.

Photocatalytic water splitting. In order to investigate the effect of morphology and type of linker on the photocatalytic performance of the samples, we have tested the hybrids for H_2 generation though sacrificial water splitting. The hybrids generally showed significantly improved H_2 evolution rates compared with pure ZnO. The respective rates of the catalysts were highly reproducible with the highest activity being observed with PCA (3 ± 0.3 μmol h^{-1} for 16 mg catalyst, corresponding to 188 μmol h^{-1} g^{-1}), which was almost twice that of the linker-free samples (1.5 ± 0.3 μmol h^{-1}, corresponding to 94 μmol h^{-1} g^{-1}, Fig. S11). This increase in activity is likely related to the aforementioned improvements in uniformity coverage of the ZnO coating. A higher coverage is expected to increase the interfacial area and so facilitate charge transfer (and thus charge separation) between the two components. This was also confirmed by preliminary photoluminescence studies (Fig S12). However, in addition to affecting the morphology of the hybrids, more detailed studies are required to reveal any further contribution of the linker molecules (i.e. active role in the charge transfer) and to reveal the rather complex reaction mechanisms in nanocarbon-inorganic hybrid photocatalysts.

Conclusions

We have coated various nanocarbon surfaces with ZnO via atomic layer deposition (ALD) and investigated the role of structural defects, covalently-attached functional groups and non-covalently adsorbed aromatic linking agents on the nucleation and growth of the ZnO crystals. In contrast to intrinsic defects and organic groups induced by acid treatment, non-covalently attached aromatic linkers were uniformly adsorbed on the entire CNT surface and thus provided a higher quantity and uniformly distributed nucleation sites. Among the three tested linker molecules, pyrene carboxylic acid (PCA) has yielded the most homogeneous and complete coating with uniform particle shape and very narrow crystal size distribution. Importantly, in contrast to benzyl alcohol (BA) and naphthalene carboxylic acid (NA), the interaction of PCA with the nanocarbon surface was also sufficiently strong to withstand desorption under high vacuum even at temperatures as high as 200 °C. Furthermore, the modification with PCA has enabled coatings on nanocarbons without the typical corrosion caused by oxidative treatments. Therefore, PCA offers a simple, versatile and non-destructive route for atomic layer deposition of metal oxides and other inorganic compounds onto a variety of carbon nanomaterials, thus providing a whole range of novel interface-dominated functional hybrid materials for environmental and sustainable energy applications.

Acknowledgements

We acknowledge the funding by the European Union's 7th Framework Program FP7/2007-2013 under grant agreement no.310184. N.K. is grateful for financial support by the Graduate School of Chemistry at the University of Münster. We further thank Paul Gebhardt for conducting HRTEM characterization of the samples, Nina Winkler for additional experimental support and Vassilios Siozios and Olga Fromm for the TGA measurements.

Notes and references

[a] Institute of Physical Chemistry, Westfälische Wilhelms-Universität, Corrensstrasse 28/30, 48149 Münster, Germany. E-mail: dominik.eder@uni-muenster.de.
[b] Institute of Materials Physics, Westfälische Wilhelms-Universität, Wilhelm-Klemm-Str.10 , 48149 Münster, Germany.
Electronic Supplementary Information (ESI) available: [details of any supplementary information available should be included here]. See DOI: 10.1039/b000000x/

1. D. Eder, *Chemical Reviews*, 2010, **110**, 1348-1385.
2. J. J. Vilatela and D. Eder, *ChemSusChem*, 2012, **5**, 456-478.
3. G. A. Rivas, M. D. Rubianes, M. C. Rodríguez, N. F. Ferreyra, G. L. Luque, M. L. Pedano, S. A. Miscoria and C. Parrado, *Talanta*, 2007, **74**, 291-307.
4. L. Dai, D. W. Chang, J.-B. Baek and W. Lu, *Small*, 2012, **8**, 1130-1166.
5. Y. Liang, Y. Li, H. Wang and H. Dai, *Journal of the American Chemical Society*, 2013, **135**, 2013-2036.
6. T. Ando, *NPG Asia Mater*, 2009, **1**, 17-21.
7. A. A. Balandin, *Nat Mater*, 2011, **10**, 569-581.
8. D. Eder and A. H. Windle, *Journal of Materials Chemistry*, 2008, **18**, 2036-2043.
9. A. S. Cherevan, P. Gebhardt, C. J. Shearer, M. Matsukawa, K. Domen and D. Eder, *Energy & Environmental Science*, 2014, **7**, 791-796.
10. S. M. George, *Chemical Reviews*, 2009, **110**, 111-131.
11. A. D. Franklin, S. O. Koswatta, D. B. Farmer, J. T. Smith, L. Gignac, C. M. Breslin, S.-J. Han, G. S. Tulevski, H. Miyazoe, W. Haensch and J. Tersoff, *Nano Letters*, 2013, **13**, 2490-2495.
12. X. Meng, M. Ionescu, M. Banis, Y. Zhong, H. Liu, Y. Zhang, S. Sun, R. Li and X. Sun, *J Nanopart Res*, 2011, **13**, 1207-1218.
13. X. Wang, S. M. Tabakman and H. Dai, *Journal of the American Chemical Society*, 2008, **130**, 8152-8153.
14. B. Lee, G. Mordi, M. J. Kim, Y. J. Chabal, E. M. Vogel, R. M. Wallace, K. J. Cho, L. Colombo and J. Kim, *APPLIED PHYSICS LETTERS*, 2010, **97**, 043107-043107-043103.
15. A. A. Dameron, S. Pylypenko, J. B. Bult, K. C. Neyerlin, C. Engtrakul, C. Bochert, G. J. Leong, S. L. Frisco, L. Simpson,

H. N. Dinh and B. Pivovar, *Applied Surface Science*, 2012, **258**, 5212-5221.
16. D. B. Farmer and R. G. Gordon, *Nano Letters*, 2006, **6**, 699-703.
17. C. J. Shearer, A. Cherevan and D. Eder, *Advanced materials*, 2014, **26**, 2295-2318.
18. J. Zhao, H. Park, J. Han and J. P. Lu, *The Journal of Physical Chemistry B*, 2004, **108**, 4227-4230.
19. X. L. Li, C. Li, Y. Zhang, D. P. Chu, W. I. Milne and H. J. Fan, *Nanoscale Research Letters*, 2010, **5**, 1836-1840.
20. X. Chen, H. Zhu, Y.-C. Chen, Y. Shang, A. Cao, L. Hu and G. W. Rubloff, *ACS NANO*, 2012, **6**, 7948-7955.
21. X. Meng, D. Geng, J. Liu, R. Li, X. Sun, *Nanotechnology*, 2011, **22**, 1-10.
22. X. Li, X. Meng, J. Liu, D. Geng, Y. Zhang, M. N. Banis, Y. Li, J. Yang, R. Li, X. Sun, M. Cai and M. W. Verbrugge, *Advanced Functional Materials*, 2012, **22**, 1647-1654.
23. C. Marichy and N. Pinna, *Coordination Chemistry Reviews*, 2013, **257**, 3232-3253.
24. D. Eder and A. H. Windle, *Advanced materials*, 2008, **20**, 1787-1793.
25. R. L. Puurunen, *JOURNAL OF APPLIED PHYSICS*, 2005, **97**, -.
26. N. Ouldhamadouche, A. Achour, I. Musa, K. Ait Aissa, F. Massuyeau, P. Y. Jouan, M. Kechouane, L. Le Brizoual, E. Faulques, N. Barreau and M. A. Djouadi, *Thin Solid Films*, 2012, **520**, 4816-4819.
27. C. Singh, M. S. P. Shaffer, K. K. K. Koziol, I. A. Kinloch and A. H. Windle, *Chemical Physics Letters*, 2003, **372**, 860-865.
28. M. Krissanasaeranee, S. Wongkasemjit, A. K. Cheetham and D. Eder, *Chemical Physics Letters*, 2010, **496**, 133-138.
29. D. J. Cooke, D. Eder and J. A. Elliott, *The Journal of Physical Chemistry C*, 2010, **114**, 2462-2470.
30. M. Cao, A. Fu, Z. Wang, J. Liu, N. Kong, X. Zong, H. Liu and J. J. Gooding, *The Journal of Physical Chemistry C*, 2014, **118**, 2650-2659.
31. X.-b. Yan, B.-k. Tay, Y. Yang and W. Y. K. Po, *The Journal of Physical Chemistry C*, 2007, **111**, 17254-17259.
32. R. Vidya Sagar and S. Buddhudu, *Physics Letters A*, 2009, **373**, 3184-3189.
33. P. Scherrer, *Nachrichten von der Gesellschaft der Wissenschaften zu Göttingen Mathematisch-Physikalische Klasse*, 1918, **1918**, 98-100.
34. U. Holzwarth and N. Gibson, *Nature Nanotechnology*, 2011, **6**, 534.